Conformational Changes during Protein Adsorption. FT-IR Spectroscopic Imaging of Adsorbed Fibrinogen Layers

ARTICLE *in* ANALYTICAL CHEMISTRY · MARCH 2007

Impact Factor: 5.64 · DOI: 10.1021/ac061341j · Source: PubMed

4 AUTHORS, INCLUDING:

Gerald Steiner
Technische Universität Dresden
72 PUBLICATIONS **732** CITATIONS
SEE PROFILE

Manfred F Maitz
Leibniz Institute of Polymer Research Dresden
114 PUBLICATIONS **1,797** CITATIONS
SEE PROFILE

Anal. Chem. **2007,** *79,* 1311−1316

Conformational Changes during Protein Adsorption. FT-IR Spectroscopic Imaging of Adsorbed Fibrinogen Layers

Gerald Steiner,*,† Sibel Tunc,†,‡ Manfred Maitz,§ and Reiner Salzer†

Institute for Analytical Chemistry, Dresden University of Technology, 01062 Dresden, Germany, and Institute of Ion Beam Physics and Material Research, Research Center Rossendorf, 01314 Dresden, Germany

The influence of hydrophobicity of the substrate surface on structural changes during protein adsorption was investigated. Plasma fibrinogen was chosen to model this effect as it is the most important protein in the body that adsorbs to foreign surfaces. Only conformations of adsorbed fibrinogen similar to that of the protein in solution do not activate the process of blood coagulation. Small spots on the substrate surface with conformational changes within the adsorbed protein are already sufficient to deteriorate biocompatibility. Mid-infrared hyperspectral imaging permits the identification of coagulated spots down to a few micrometers in size. The spectra of the FT-IR images that were assessed to be of suitable quality were clustered by a fuzzy c-means algorithm. The determination of the appropriate number of clusters was based on cluster variance. Subsequent evaluation of the centroid spectra of each cluster showed that their amide I band was separated into contributions from different structural units, with the α-helix content always being dominant. Significant differences between hydrophobic and hydrophilic surfaces were observed for turn and sheet contributions. Lower sheet/turn ratios appear to indicate inferior biocompatibility. Spots on hydrophilic surfaces could be identified, which exhibit structural changes similar to those on hydrophobic surfaces.

Adsorption of proteins is a key event whenever a surface is exposed to biological fluids. Important examples are biosensors or implants, whose application range is often restricted due to protein adsorption. Because plasma fibrinogen is the most relevant protein in the body that adsorbs to foreign material surfaces, it was selected for this method development. Fibrinogen takes part in blood coagulation and facilitates adhesion as well as aggregation of platelets, which are very important properties in the processes of both hemeostasis and thrombosis.[1] Human plasma fibrinogen is a 340-kDa dimeric protein, the molecular structure of which is shown schematically in Figure 1A. The protein consists of two peripheral D domains and one central E domain linked together by triple-stranded α-helical coiled coils. In this extended trinodular model composed of globular and coiled-coil regions, the N termini of all six α, β, and γ chains fold in the central E domain. The C termini of the longer α chains turn back toward the central E domain, whereas the C termini of the β and γ chains fold within the D domains. According to the current understanding, the C termini of β and γ chains fold independently in separate domains (Figure 1B).[2]

The adsorption of fibrinogen is a complex process involving noncovalent interactions, electrostatic forces, hydrogen bonding, and van der Waals forces.[3] The precise molecular mechanism of fibrinogen adsorption is not yet fully understood. According to the current understanding, the D and E domains tend to interact with the material surface once fibrinogen adsorbs to foreign-body material. The material surface then promotes conformation changes within the D and E domains and the release of fibrinopeptides.[4,5] Substrate properties such as surface energy, surface roughness, and surface chemistry have been identified as key factors influencing the structure of adsorbed fibrinogen.[6] In particular, the hydrophobicity of the surface has a strong influence.[7] For fibrinogen adsorbed on hydrophobic mica, an extended, slightly curved shape of a mean length of 65.9 nm and a mean diameter of 3.4 nm was reported.[8] On hydrophilic quartz, fibrinogen molecules appear in a form of a trinodular rod of a mean length of 46 nm and a mean diameter of 4 nm.[9]

Once fibrinogen has covered the surface of implants, host cells are no longer able to contact the underlying foreign-body material but only the protein-coated surface. This adsorbed protein layer—rather than the foreign material itself—may stimulate or inhibit further biochemical processes. If conformational changes occur,

* To whom correspondence should be addressed. E-mail: gerald.steiner@chemie.tu-dresden.de.

† Dresden University of Technology.

‡ Present address: Department of Chemistry, Akdeniz University, 07058 Antalya, Turkey.

§ Research Center Rossendorf.

(1) Cacciafesta, P.; Humphris, A. D. L.; Jandt, K. D.; Miles, M. J. M. *Langmuir* **2000**, *16*, 8167−8175.

(2) Hall, C. E.; Slayter, H. S. *J. Biophys. Biochem. Cytol.* **1959**, *5*, 11−16.

(3) Jung, S. Y.; Lim, S. M.; Albertorio, F.; Kim, G.; Gurau, M. C.; Yang, R. D.; Holden, M. A.; Cremer, P. S. *J. Am. Chem. Soc.* **2003**, *125*, 12782−12786.

(4) Tang, L.; Ugarova, T. P.; Plow, E. F.; Eaton, J. W. *J. Clin. Invest.* **1996**, *97*, 1329−1334

(5) Tang, L. *J. Biomater. Sci. Polym.* **1998**, *9*, 1257−1266.

(6) Weber, D.; Bolikal, S. L.; Bourke, J.; Kohn, J. *Biomed. Mater. Res.* **2004**, *68A*, 496−503.

(7) Wertz, C. F.; Santore, M. M. *Langmuir* **2002**, *18*, 706−715.

(8) Taatjes, D. J.; Quinn, A. S.; Jenny, R. J.; Hale, P.; Bovill, E. G.; McDonagh, J. *Cell Biol. Int.* **1997**, *21*, 715−726.

(9) Wigren, R.; Elwing, H.; Erlandsson, R.; Welin, S.; Lundstrom, I. *FEBS Lett.* **1991**, *280*, 225−228.

10.1021/ac061341j CCC: $37.00
Published on Web 01/10/2007

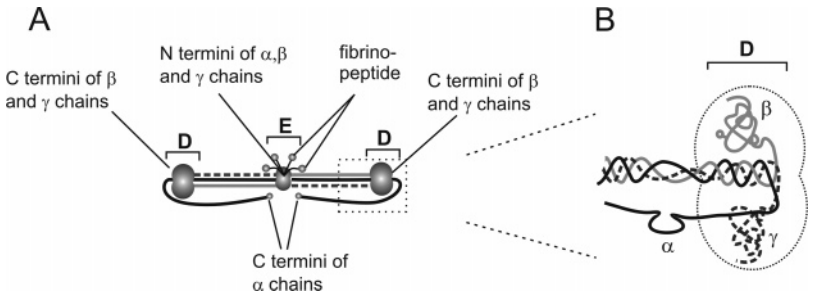

Figure 1. (A) Sketch of the total molecular organization of human plasma fibrinogen. (B) More detailed view on the peptide chains in the D domain.

adsorbed fibrinogen may either trigger interaction with other fibrinogen molecules forming a fibrin web or initiate the subsequent adsorption of phagocytes. Thus, properties of the adsorbed fibrinogen critically determine the biocompatibility of a substrate. The conformation of adsorbed fibrinogen is commonly used as a biocompatibility indicator.[10] Understanding the influence of the biomaterial's surface chemistry on the conformation of adsorbed proteins is crucial for improvement of the biocompatibility of foreign-body materials.[11,12] In particularm the surface of endovascular devices, which are in direct contact with blood flow, must not activate the tissue or the blood cell reaction to foreign bodies. Compatibility features can be improved by surface modification or by covering with biocompatible coatings.[13] One approach to improve the biocompatibility of endovascular devices is the surface passivation by preadsorbed fibrinogen in such a conformation that blood coagulation will not be activated.

Current investigations are focused on the characterization of adsorbed fibrinogen by Fourier transform infrared (FT-IR) spectroscopy,[14] atomic force microscopy,[15] ellipsometry,[16] neutron reflection spectroscopy,[17] Raman spectroscopy,[18] and total internal reflectance fluorescence spectroscopy.[19] FT-IR spectroscopy has sufficient sensitivity to examine the structure of proteins in solution[20,21] and even on surfaces.[22,23] Mid-infrared spectra of proteins exhibit several amide bands. The amide I band (1600−1700 cm^{-1}) is mostly used to extract information about the secondary structure. Because each of the different secondary structural elements contributes to the infrared spectrum, the observed amide bands are composed of several overlapping components representing α-helix, sheet, turn, and random structures.[24] The amide I vibration comprises contributions from the C═O stretching vibration of the amide group (80%), the in-plane N−H bending, and the C−N stretching modes. The exact frequency of the amide I vibration depends on the nature of the hydrogen bonding between C═O and N−H groups, which is in turn determined by the particular secondary structure adopted by the protein.

The present study demonstrates that FT-IR imaging spectroscopy is a useful tool to characterize changes in the conformation of adsorbed fibrinogen. It allows the homogeneity of a protein-covered surface to be imaged. Such surfaces may play an important role in the development of new material with advanced biocompatibility. A current idea to improve the biocompatibility of an artificial blood vessel is the preadsorption of fibrinogen. The challenge consists in the generation of adsorbed fibrinogen layers of desired conformation that inhibit blood coagulation. It was already demonstrated by conventional FT-IR microspectroscopy that human plasma fibrinogen undergoes changes in secondary structure upon adsorption on surfaces of different hydrophobicity.[25] Unfortunately, such integral data are not sufficient to assess biocompatibility. Small spots of insufficient biocompatibility within an otherwise perfect surface area may not contribute much to the total conformation distribution, but they are certainly sufficient to initiate the coagulation cascade. Such small spots of insufficient biocompatibility may accidentally be revealed by conventional FT-IR microspectroscopy. However, a reliable assessment of the biocompatibility of the complete surface requires imaging techniques. FT-IR imaging spectroscopy combines the high sensitivity for conformational analysis with a spatial resolution down to a few micrometers. The analysis of adsorbed fibrinogen layers on hydrophobic and hydrophilic silicon surfaces by FT-IR imaging spectroscopy is the objective of the present study. Silicon was chosen because of (i) its optical properties in the IR range and (ii) its chemical properties, which permit the formation of hydrophobic or hydrophilic surfaces without changing the substrate itself.

MATERIALS AND METHODS

Silicon wafers of (100) crystal orientation, n-doped with As (SilChem, Freiberg, Germany) were cut into squares of ~10 × 10 mm^2. The substrates were oxidized in a 1:1 mixture of H_2SO_4

(10) Salzman, E. W.; Linden, J.; McManama, G.; Ware, J. A. *Ann. N. Y. Acad. Sci.* **1987**, *516*, 184−195.
(11) Agashe, M.; Raut, V.; Stuart, S. J.; Latour, R. A. *Langmuir* ***2005***, *21*, 1103−1117.
(12) Weber, N.; Wendel, H. P.; Kohn, J. *J. Biomed. Mater. Res.* **2005**, *72A*, 420−427.
(13) Prunotto, M.; Galloni, M. *Anal. Bioanal. Chem.* **2005**, *381*, 531−533.
(14) Müller, M.; Werner, C.; Grundke, K.; Eichhorn, K. J.; Jacobasch, H. J. *Microcim. Acta Suppl.* **1997**, *14*, 671−674.
(15) Bergkvist, M.; Carlsson J.; Oscarsson, S. *J. Biomed. Mater Res.* **2003**, *64A*, 349−356.
(16) Malmsten, M. *Colloids Surf., B* **1995**, *3*, 371−381.
(17) Armstrong, J.; Salacinski, H. J.; Mu, Q.; Seifalian, A. M.; Peel, L.; Freeman, N.; Holt, C. M.; Lu, J. R. *J. Phys. Condens. Matter.* **2004**, *16*, 2483−2492.
(18) Strehle, M. A.; Roesch, P.; Petry, P.; Hauck, A.; Thull, R.; Kiefer, W.; Popp, J. *Phys. Chem. Chem. Phys.* **2004**, *6,* 5232−5236.
(19) Shibata, C. T.; Lenhoff, A. M. *J. Colloid Interface Sci.* **1992**, *148*, 485−507.
(20) Sarver, R. W., Jr.; Krueger, W. C. *Anal. Biochem.* **1991**, *194*, 89−100.
(21) Dong, A.; Caughey. W. S.; Du, Clos, T. W. *J. Biol. Chem.* **1994**, *269*, 6424−6430.
(22) Buijs, J.; Norde, W.; Lichtenbelt, J. W. Th. *Langmuir* **1996**, *12*, 1605−1613.
(23) Cheng, S. S.; Chittur, K. K.; Sukenik, C. N.; Culp, L. A.; Lewandowska, K. *J. Colloid Interface Sci.* **1994**, *162*, 135−143.
(24) Giacomelli, C. E.; Bremer, M. G. E. G.; Norde, W. *J. Colloid Interface Sci.* **1999**, *220*, 13−23.
(25) Tunc, S.; Maitz, M. F.; Steiner, G.; Vazquez, L.; Pham, M. T.; Salzer, R. *Colloids Surf., B* **2005**, *42,* 219−225.

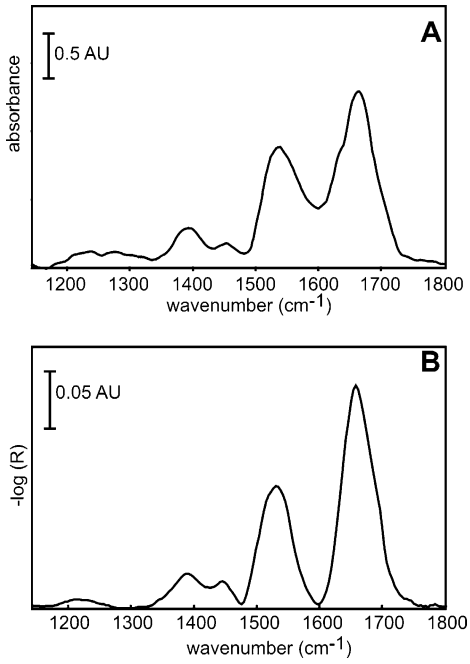

Figure 2. (A) FT-IR spectrum of fibrinogen solution and (B) FT-IR reflection spectrum of fibrinogen adsorbed to a hydrophobic Si surface.

and 30% H_2O_2 for 20 min, subsequently sonicated 10 min in acetone and ethanol, then boiled in water for 1 h, and finally sonicated in water for 10 min. Some surfaces were further treated with 5% HF for 1 min to obtain surfaces that differ in their surface energy. Contact angles were measured using an instrument DSA10/DO 3020 (Krüss GmbH, Hamburg, Germany) and the sessile drop method with 2 μL of water for the characterization of the surfaces.

Silicon substrates with hydrophobic and hydrophilic surfaces were immersed in 2 mg/mL solutions of fibrinogen fraction I (type IV from bovine plasma, Sigma, Taufkirchen, Germany) in phosphate-buffered saline at pH 7.4 for 60 min. Substrates were then removed from the solution, rinsed with deionized water, and dried in a slow flow of dry air.

FT-IR spectroscopic images were collected in the external reflection mode using a Bruker FT-IR imaging spectrometer Hyperion (Bruker Optik GmbH, Ettlingen, Germany) coupled to an IR microscope (IRscope, Bruker Optik GmbH). The imaging detector was a 64 × 64 mercury−cadmium telluride focal plane array detector (Santa Barbara Research, Santa Barbara, CA.) The 15-fold Cassegrainian objective with a numerical aperture of 0.4 imaged a sample area of ~270 × 270 μm^2. A low-pass filter with a cutoff at the Nyquist frequency was inserted into the beam to eliminate radiation of unwanted wavelengths and prevent Fourier foldover perturbations as well as to reduce the size of the spectroscopic data cube. Reference spectroscopic images were captured from neat silicon wafers. A total of 51 interferograms were coadded for each of the 4096 image pixels of every sample. The interferograms were Fourier transformed applying Happ-Genzel apodization, and no zero filling was applied. The ratios of spectra at a resolution of 4 cm^{-1} of the sample image against the spectra of the reference image were taken and transferred to absorbance values. In order to obtain a signal-to-(peak-to-peak) noise ratio of >50, the measurements were repeated 5 times and

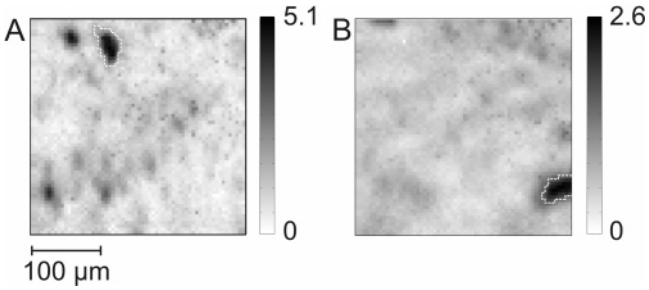

Figure 3. FT-IR spectroscopic images of fibrinogen adsorbed to (A) a hydrophobic and (B) a hydrophilic surface. The images were collected in reflection mode. Each pixel gives the gray-coded integrated absorbance value in a spectral range from 1150 to 1800 cm^{-1}. The dashed lines indicate areas of strongest protein adsorption.

finally the absorbance spectra for each pixel were averaged. The frame rate of the camera was 126 Hz, yielding a total measurement time of ~100 min for each sample. Data preprocessing and image processing were carried out using the MatLab Package (Version 7, MathWorks Inc. Natric, MA).

RESULTS AND DISCUSSION

Surface chemistry plays a key role in the conformational changes that a protein undergoes upon adsorption on a biomaterial surface. Here we chose two types of surface-treated silicon.[25] Initially both types were oxidized, and the second type underwent additional HF treatment. The hydrophobicity of both substrates was checked by contact angle experiments. The oxidized Si surface has a contact angle of 27.7° ± 3.05°, and the Si surface after HF treatment has a contact angle value of 5.0° ± 1.72°. Such very low contact angles indicate highly hydrophilic surfaces. The decrease in contact angle is caused by an increase of negatively charged ions (F^- and OH^-) on the surface after the HF etching process. We will refer to the non-HF-treated substrate as hydrophobic and the HF-treated substrate as hydrophilic.

FT-IR spectra (spectral range from 1150 to 1800 cm^{-1}) of fibrinogen in solution (20 mg/mL) and adsorbed on a hydrophobic surface are shown in Figure 2. The spectra exhibit characteristic bands that result primarily from vibrations in the peptide linkages. The two dominant amide bands appear around 1650 (amide I band) and 1550 cm^{-1} (amide II band). The bands at 1460 and 1390 cm^{-1} are assigned to the CH_2 deformation and to vibrations of the amino acid side chains, respectively. The amide III band is located at 1220 cm^{-1}. Differences in the band shape of the amide I and amide II bands are obvious.

FT-IR spectroscopic images of adsorbed fibrinogen to hydrophobic and hydrophilic surfaces are shown in Figure 3. Each image covers a sample area of 270 μm × 270 μm. For every pixel, the integral intensity across the spectral range 1150−1800 cm^{-1} is transformed to a gray value. The darker the pixel, the higher is the surface concentration of fibrinogen. The layers of adsorbed fibrinogen are inhomogeneously distributed across the surfaces. It should be noted that fibrinogen is even adsorbed in the brightest (light gray) areas. The two domains exhibiting strongest adsorption are enclosed by dashed lines. We shall refer to these domains in the discussion further down.

Since Figure 3 was computed from integrated intensities, it does not reveal structural properties of fibrinogen in different spots of the surface. Such structural properties can be accessed by

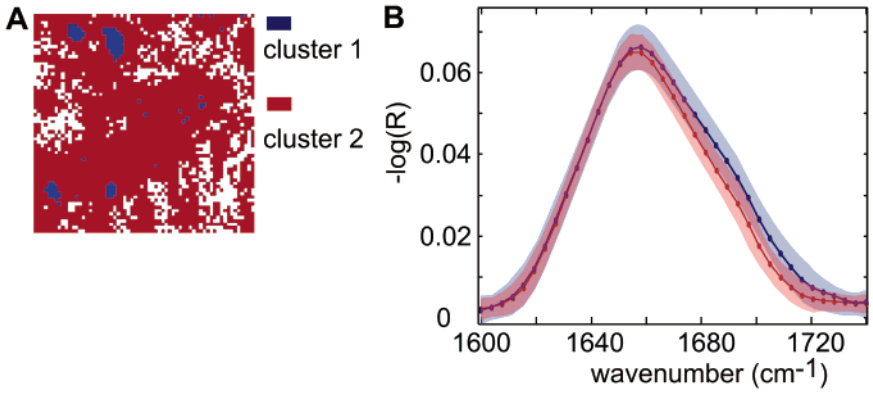

Figure 4. Fuzzy c-means cluster analysis of the data set with two clusters preselected. (A) Map of the distribution of the two clusters. Size of the map is 270 μm $\times$ 270 μm. White pixels indicate spectra that did not pass the quality assessment. (B) Centroid spectra of the two clusters (solid lines) and their variance (colored range).

separating the structure-specific contributions to the amide I band and by evaluating each component band individually.[26] Because spectroscopic images comprise thousands of individual spectra, their evaluation requires automated processing. The initial step of this automated processing is quality assessment for each single spectrum. Spectra with a maximum of the amide I band complex lower than 0.01 absorbance unit were considered as outliers and removed from the data sets. Discarded spectra are displayed as white spots in the subsequent maps. All accepted spectra were normalized to their integral absorbance in order to eliminate bias in the structure elucidation due to varying surface concentration. Subsequently, a Matlab fuzzy c-means cluster algorithm[27] was used to distribute the spectra into a number of clusters because cluster analysis is more stable than other methods of multivariate analysis such as principal component analysis.[28]

At this stage, the preselection of the number of clusters is required. This is a critical decision since different numbers of clusters may lead to different results. Unfortunately, the correct number of clusters is often not known in advance.

The problem of finding the appropriate number of clusters is usually called cluster validity.[29] Several validation criteria have been proposed for the evaluation of clustering results.[30,31] Most of these methods perform satisfactorily if the variance within a cluster is small and the clusters do not overlap.[32] In spectroscopic data sets, however, overlapping of clusters as well as noise and outliers are common. For this reason, the expected number of clusters is either simply estimated in spectroscopic data analysis[33] or the number of clusters is first overspecified and compatible clusters are subsequently merged.[34] These approaches are appropriate if the number of clusters within the spectroscopic data

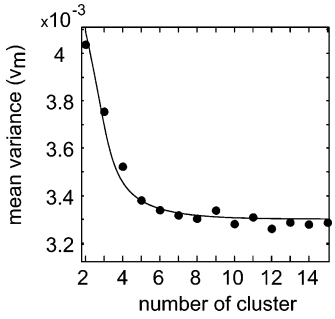

Figure 5. Mean variance (dots) for all clusters versus number of preselected clusters. The solid line was approximated by a Taylor series.

set is known or can reasonably be estimated. If insufficient prior knowledge about the number of clusters is available, one may choose various numbers of clusters and select the "best" result by common sense.[35] Too often the latter approach is biased. In the case of adsorbed protein, it is usually not possible to estimate the number of existing conformers or how many of them can be discriminated by IR spectroscopy. Cluster properties like variance within clusters or distance between clusters may be exploited here in order to validate the optimal number of clusters[36] In this study, we chose cluster variance, because it reveals the scattering of the experimental data within the cluster.

The chosen method to select an optimal number of clusters is demonstrated on an example with two preselected clusters. Figure 4A shows the result of fuzzy c-means cluster analysis of the spectral data set in Figure 3A. The clustering was performed for the amide I band in the spectral range from 1600 to 1740 cm^{-1}. The spectra belonging to these two clusters are collected in Figure 4B. The two solid lines represent the centroid spectra of the clusters. Centroid spectra are averages over all spectra in the cluster; i.e., centroid spectra indicate the cluster center. Variance within all spectra of a particular cluster can be expressed for every centroid spectral data point. The variances within the two clusters are indicated by red and blue areas around the centroid spectra. Variances in this particular data set range between 0.002 and 0.0045 [ordinate units]^2. In Figure 4B, the differing cluster properties are revealed by the distance in the centroid spectra all

(26) Jackson, M.; Mantsch, H. H.; *Crit. Rev. Biochem. Mol. Biol.* **1995**, *30*, 95−120.
(27) Vandeginste, B. G. M.; Massart, D. L.; Buydens, L. M. C.; De Jong, S.; Lewi, P. J.; Smeyers-Verbeke, S. *Data handling in science and technology Part B*; Elsevier: Amsterdam, 1989.
(28) Diem, M.; Romeo, M.; Boydston-White, S.; Milkvic, M.; Matthäus, C. *Analyst* **2004**, *129*, 880−885.
(29) Yang, M. S.; Wu, K. L. *Pattern Recognit.* **2005**, *39*, 5−21.
(30) Kwon, S. H. *Electron. Lett.* **1998**, *34*, 2176−2177.
(31) Zahid, N.; Limouri, M.; Essaid, A. *Pattern Recognit.* **1999**, *32*, 1089−1097.
(32) Sun, H.; Wang, S.; Jiang, Q. *Pattern Recognit.* **2004**, *37*, 2027−2037.
(33) Mansfield, J. R.; Sowa, M. G.; Scarth, G. B.; Somorjai, R. L.; Mantsch, H. H. *Anal. Chem.* **1997**, *69*, 3370−3374.
(34) Frigue, H.; Krishnapuram, R. *Pattern Recognit. Lett.* **1996**, *17*, 1223−1232.
(35) Naes, T.; Mevik, B. H. *J. Chemom.* **1999**, *13*, 435−444.
(36) Kim, D. W.; Lee, K. H.; Lee, D. *Pattern Recognit.* **2004**, *37*, 2009−2025.

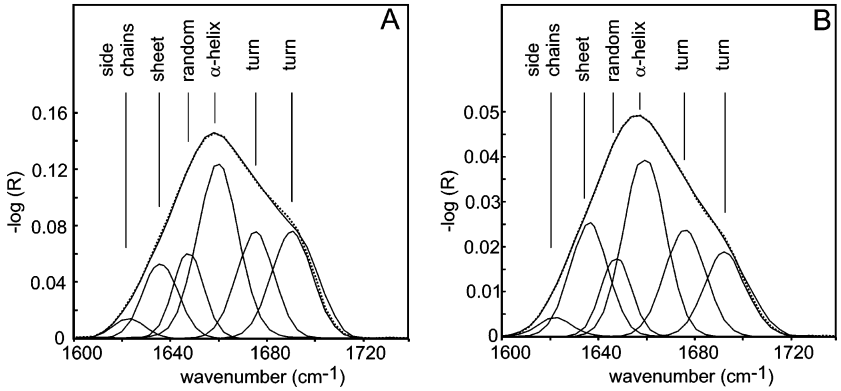

Figure 6. Separation of the amide I band of fibrinogen into its structural components. (A) Fibrinogen adsorbed to a hydrophobic Si surface and (B) fibrinogen adsorbed to a hydrophilic Si surface. In both cases, the sum of the separated band components (dotted curve) fits the measured band contour (solid line) very well.

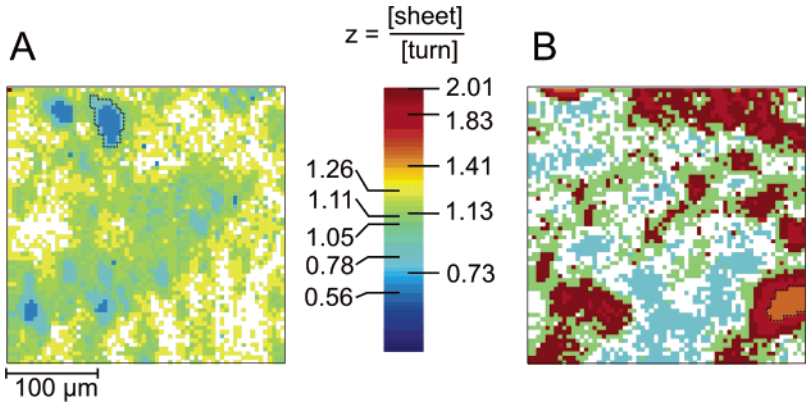

Figure 7. Color-coded [sheet]/[turn] ratios and their distribution (A) for fibrinogen adsorbed to a hydrophobic Si surface and (B) for fibrinogen adsorbed to a hydrophilic Si surface. White pixels indicate spectra that did not pass the quality assessment. The dashed lines encompass the same areas as in Figure 3. The exact values of the [sheet]/[turn] ratios for the centroid spectra of the corresponding five clusters are indicated at the color bar.

over the high-wavenumber side of the amide I band. In terms of variance, the strongest differences are found around 1686 cm^{-1} and around 1706 cm^{-1}.

When the preselected number of clusters in the example above is increased, spectra can probably be assigned more homogeneously; hence, the variance of the centroid spectra should decrease. This holds as long as additional clusters represent real features. From the point of view of information theory, variances reach a minimum as soon as the number of clusters is equal to the number of those features that can be distinguished from the spectroscopic data set.[37] Further increase of the number of clusters does not result in smaller variances. The homogeneity within clusters does not improve; only the assignment of spectra to particular clusters varies.

In Figure 4B, the variance is not constant across the investigated spectral range. In order to evaluate the influence of the preselected number of clusters on the variance, the mean variance v_m has to be computed across all C clusters and all ν wavenumbers.

$$V_m = \sum_C \sum_\nu V_{C,\nu} \quad (1)$$

Figure 5 displays v_m versus the number of clusters C, again for the data set of Figure 3A. Initially, the mean variance drops rapidly as the number of clusters increases followed by an almost horizontal region of the curve. The optimal number of clusters is found at the transition between the steep decay and the almost horizontal region. We employed a Taylor series expansion in order to fit the data in Figure 5. The apex of the approximated function is located at $C = 4.7$. Any larger number of clusters ($C > 5$) would not result in significantly lower variance or improved information retrieval. Similar results were obtained for the spectra of the other data sets. All spectra within one cluster are very similar as long as the optimal number of clusters—optimal with respect to v_m—was chosen. Since the centroids are mean spectra of a cluster, they exhibit a signal-to-noise ratio superior to each individual spectrum within the cluster. We chose the centroid spectra for the subsequent evaluation.

The amide I band complex evaluated here comprises contributions from secondary structural elements in the protein.[38] The integral intensity of each component band is a measure of the abundance of the corresponding secondary structure element (Figure 6). The curve-fitting procedure employed to separate the

(37) Henrion, R.; Henrion, G. *Multivariate Datenanalyse*; Spinger Verlag: Berlin, 1995.
(38) Sonoyama, M.; Miyazawa, M.; Katagiri, G.; Ishida, H. *Appl. Spectrosc.* **1997**, *51*, 545−547.
(39) Spraggon, G.; Everse, S. J.; Doolittle, R. F. *Nature* **1997**, *389*, 455.
(40) Haynes, C. A.; Norde, W. *Colloids Surf., B* **1994**, *2*, 517−566.
(41) Sagvolden, G.; Giaever, I.; Feder, J. *Langmuir* **1998**, *14*, 5984−5987.

contributions by each secondary structure element of the adsorbed fibrinogen has already been proven for conventional measurements of adsorbed fibrinogen.[25] The procedure was always carried out in the same way in order to allow comparison between the centroid spectra. Band positions used as input parameters are as follows:

sheet	random	α-helix	turn	turn
$1633 \pm 2\ cm^{-1}$	$1647\ cm^{-1}$	$1658 \pm cm^{-1}$	$1675 \pm 2\ cm^{-1}$	$1689 \pm 2\ cm^{-1}$

An additional band around $1620\ cm^{-1}$ is assigned to side chains. It had to be included in the band-fitting procedure but will not be considered in the discussion of the secondary structures. Full widths at half-height of $10\ cm^{-1}$ and Gaussian shape were assumed for each component band.[21] The Gaussian shape was chosen according to the literature.[23] Representative results for curve fitting of the amide I band of the data sets in Figure 3 are given in Figure 6. In both cases, α-helices exhibit the most dominant absorption bands. Significant differences between the hydrophobic surface (Figure 6A) and the hydrophilic surface (Figure 6B) are observed for sheet and turn contributions. As the growth of the component band at $1633\ cm^{-1}$ indicates, the amount of sheet clearly increases on the hydrophilic surface. Simultaneously, the turn contribution decreases as indicated by the reduced band size at $1689\ cm^{-1}$. It was already reported that sheet regions in C-terminal domains of β and γ chain respond sensitively to changes of surrounding conditions.[39]

The distribution of the ratio z of sheet and turn across the sample surface is calculated from the integrated intensities of the corresponding component bands (sheet, $1633\ cm^{-1}$; turn, 1675 and $1689\ cm^{-1}$):

$$\mathbf{Z} = \frac{\mathbf{A}_{1633}}{\mathbf{A}_{1675} + \mathbf{A}_{1689}} \qquad (2)$$

The distribution of z across the sample surface is depicted in Figure 7A for a hydrophobic surface and in Figure 7B for a hydrophilic surface. White pixels indicate spectra that did not pass the quality assurance step in the automated evaluation procedure (cf. Materials and Methods). Higher z values (red to yellow pixels) indicate elevated sheet abundance and superior blood compatibility; lower z values (green to blue pixels) point to increasing turn abundance and inferior blood compatibility.

Fibrinogen adsorbs in general more strongly to hydrophobic surfaces than to hydrophilic ones.[40,41] This was confirmed by the data shown in Figure 3, where the maximum intensity of fibrinogen adsorbed on the hydrophobic surface (Figure 3A) is roughly twice as high as on the hydrophilic surface (Figure 3B). Upon adsorption, fibrinogen undergoes conformational changes toward a lower [sheet]/[turn] ratio, which indicates inferior blood compatibility. Blue and green pixels across the hydrophobic sample surface in Figure 7A reveal these conformation changes. Shades of blue and green dominate the hydrophobic surface.

The location of blue pixels in Figure 7A corresponds very well to spots of enhanced fibrinogen absorption in Figure 3A. The contours of the dashed lines in Figures 3A and 7A are identical. The dashed line encloses the area of highest surface concentration. In multilayers, the adsorbed fibrinogen adopts a polycrystalline structure, and as a consequence thereof, changes in secondary structure occur .[42]

Pixels with high [sheet]/[turn] ratio (superior blood compatibility) are only found in Figure 7B. The majority of pixels in Figure 7B are red, but blue and green clusters occur as well. Spot sizes of the blue clusters in Figure 7B range between 20 and 100 μm. Blue pixels cover only 22% of the total surface. As in Figure 7A, the dashed lines in Figures 3B and 7B indicate the area of highest surface concentration. On the hydrophobic surface, the amount of turn increases also with the amount of fibrinogen adsorbed. But in contrast to the hydrophilic surface, the amount of turn does not dominate within the area of highest fibrinogen adsorption. Red pixels indicate good blood compatibility even within this area. IR spectroscopic images provide the lateral resolution necessary to resolve this juxtaposition. Moreover, IR spectroscopic images provide a unique tool for the optimization of the biocompatibility of surfaces.

CONCLUSIONS

FT-IR spectroscopic images revealed the influence of the hydrophobicity of the surfaces on the structural properties of adsorbed fibrinogen. Fibrinogen on hydrophobic surfaces comprises a higher amount of turn than sheet; hence, the hydrophobic surface exhibits low blood compatibility. Hydrophilic surfaces generally exhibit superior blood compatibility. This behavior is also consistent with other reports, which demonstrated that fibrinogen on hydrophilic surfaces retains a secondary structure, which inhibits the coagulation and adsorption of cells resulting in high blood compatibility. However, FT-IR spectroscopic images reveal several spots within the adsorbed fibrinogen layer that exhibit poor blood compatibility. Such coagulation spots shall reduce the biocompatibility of the material drastically.

The results obtained by FT-IR spectroscopic imaging indicate that thin layers of adsorbed fibrinogen can reliably be characterized and—more importantly—spots of structural changes within larger sample areas can be identified and quantified. Information of this kind is crucial for the improvement of the biocompatibility of material surfaces.

ACKNOWLEDGMENT

The support of DAAD (German Academic Exchange Service) and Rossendorf Research Center to S.T. is gratefully acknowledged. The authors gratefully acknowledge Dr. M. T. Pham from the Research Center Rossendorf (Germany) for assistance with the preparation of fibrinogen layers. The authors thank the Management Unit of Scientific Research Projects of Akdeniz University.

Received for review July 24, 2006. Accepted December, 4, 2006.

AC061341J

(42) Nygren, H.; Stenberg, M.; Karlsson, C. *J. Biomed. Mater. Res.* **1992**, *26*, 77−91.